International Journal of Steel Structures 15(4): 797-807 (2015)
DOI 10.1007/s13296-015-1203-9
ISSN 1598-2351 (Print)
ISSN 2093-6311 (Online)

International Journal of
STEEL
STRUCTURES
www.springer.com/journal/13296

Experimental Study and Parameter Analysis of L-shaped Composite Column under Axial Loading

Ting Zhou[1,3], Minyang Xu[1], Xiaodun Wang[1,2,*], Zhihua Chen[1], and Ying Qin[1]

[1]*Tianjin University, Tianjin, 300072, China*
[2]*Tianjin Key Laboratory of Civil Engineering Structure and New Materials, Tianjin University, Tianjin, 300072, China*
[3]*Tianjin Key Laboratory of Architectural Physics and Environmental Technology, Tianjin University, Tianjin, 300072, China*

Abstract

A special-shaped column composed of concrete-filled steel tubes (SCFST column) is experimentally investigated in this paper. The SCFST column is composed of several small-sized concrete-filled square tubular columns (mono-columns) connected by connection plates. This kind of column is proposed because it can increase the usable space in residential buildings. The axial loading behavior of L-shaped SCFST columns is experimentally investigated. The failure mode, strain distribution, cooperation of mono-columns, bearing capacity, and the effect of a concrete core on column behavior were tested. As concluded, the SCFST column can be regarded as a useful kind of column. A finite element analysis model was proposed according to the experimental results, and the influence of connection plate size on bearing capacity was studied using the finite element model. Finally, proposed were the optimal width and thickness of connection plates for improving the design of the SCFST column.

Keywords: L-shaped column, concrete-filled steel tube, composite columns, axial loading test, finite element analysis

1. Introduction

A special-shaped column composed of concrete-filled steel tubes (SCFST column) has three types of cross-sections: L-, T-, and crisscross-shaped. An L-shaped SCFST column is composed of three small-sized concrete-filled square tubular columns called mono-columns; a T-shaped SCFST column is composed of four of these mono-columns. The mono-columns are connected by connection plates and are embedded in walls, as shown in Fig. 1. In most cases, an L-shaped column can meet universal demands for structures, making it a priority option for designers. The width of mono-columns is always smaller than the thickness of walls, allowing SCFST columns to be embedded in walls and allowing these to be hidden in room corners. In this way, the usable areas of buildings with SCFST columns are always larger than that of buildings with typical rectangular columns. The mono-column of an SCFST column is an economical concrete-filled steel tubular (CFST) column with high strength and large damping capacity (Han *et al.*, 2008). Steel tubes limit the lateral deformation of concrete and in turn, the concrete core can prevent the steel tube from buckling to a certain extent.

Special-shaped columns have been studied extensively over the past decades. Most studies have focused mainly on the static behavior of concrete special-shaped columns subjected to bi-axial eccentric load (Cheng and Thomas, 1989; Dundar and Sahin, 1993; Gao *et al.*, 2005; Joaquin, 1979; Mallikarjuna and Mahadevappa, 1992). For reinforced concrete special-shaped columns, the capacity to resist cracks and seismic capacity are critical issues (Han, 2002; Han *et al*., 2008; Yang *et al.*, 2009). CFST columns have recently attracted considerable attention for their high stiffness, ductility, and earthquake resistance (Yang *et al.*, 2010; Guo *et al*., 2012). Many kinds of special-shaped CFST columns have been proposed. Shen *et al.* (2013) investigated the seismic behavior of concrete-filled L-shaped steel tube columns (CFLST). The CFLST columns were found to exhibit favorable energy dissipation and ductility, even for the columns subjected to high axial load.

Several studies have been conducted to investigate the behavior of SCFST columns. Chen *et al.* (2006, 2009) investigated six SCFST columns under axial load and developed a superposition method to evaluate the ultimate capacity of such columns. Zhou *et al.* (2010) experimentally investigated the behavior of SCFST columns subjected to

Received September 18, 2014; accepted May 5, 2015;
published online December 31, 2015

*Corresponding author
Tel: +86-138-2058-9039, Fax: +022-27409933
E-mail: maodun2004@126.com

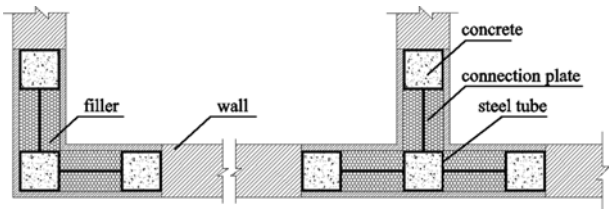

Figure 1. SCFST columns.

Figure 2. Photo of an SCFST column structure.

constant axial load and cyclically varying flexural load. Given the consideration for many details of this kind of structure, the design approach for SCFST column structures has been developed (Chen *et al.*, 2011). A SCFST column structure is shown in Fig. 2. Although some investigations have reported on the static behavior of SCFST columns, its seismic behavior has seldom been studied.

This paper investigates the axial loading behavior of L-shaped SCFST columns. Two specimens were tested to study the effect of a concrete core on column behavior. The test results were compared with those from finite element analysis. According to these results, a mathematical model was proposed to develop an analytical approach.

2. Experimental Program

2.1. Introduction

An experimental study was performed to assess the response of L-shaped SCFST columns under axial compression. Two specimens were investigated: one with concrete-filled steel tubes and one without. The main objective of the test was to study the deformation process and failure modes of SCFST columns. The effect of the concrete cores on the behavior of columns was examined. According to the test results, a finite element model was developed.

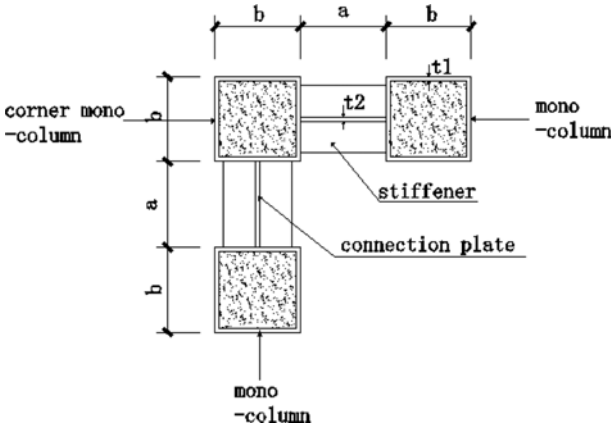

Figure 3. Details of specimens.

2.2. Specimens

Details of the SCFST column specimens are shown in Fig. 3. Both the connection plates and stiffeners were welded to the steel tubes. Table 1 provides a summary of the specimen details. Specimen S-1 was composed of hollow steel tubes. Specimen S-2 was composed of steel tubes filled with concrete; the compressive strength of this concrete was 25 MPa. The material properties of steel were determined using tensile tests on coupons extracted from the steel tubes. For the concrete, cube and cylinder tests were performed. The results of material tests are listed in Tables 2 and 3. Two steel plates with a thickness of 40 mm each were welded to the top and bottom of the specimens.

Table 1. Summary of specimens

Specimen	b (mm)	a (mm)	t_1 (mm)	t_2 (mm)	A_y (mm^2)	A_c (mm^2)	f_y (MPa)	f_c (MPa)	l (mm)
S-1	100	150	4	3	1,536	-	269	-	1,500
S-2	100	150	4	3	1,536	8,464	269	17.336	1,500

Table 2. Properties of steel tube and connection plate

Steel	t (mm)	f_y (MPa)	f_u (MPa)	E_s (MPa)	ε_y (μ)
Connection plate	3.00	312	426	148,261	2,104
Steel tube	3.75	269	445	208,305	1,291

Table 3. Properties of concrete

Concrete grade	f_{cu} (MPa)	f_c (MPa)	E_c (MPa)
C25	23.2	17.336	19,373

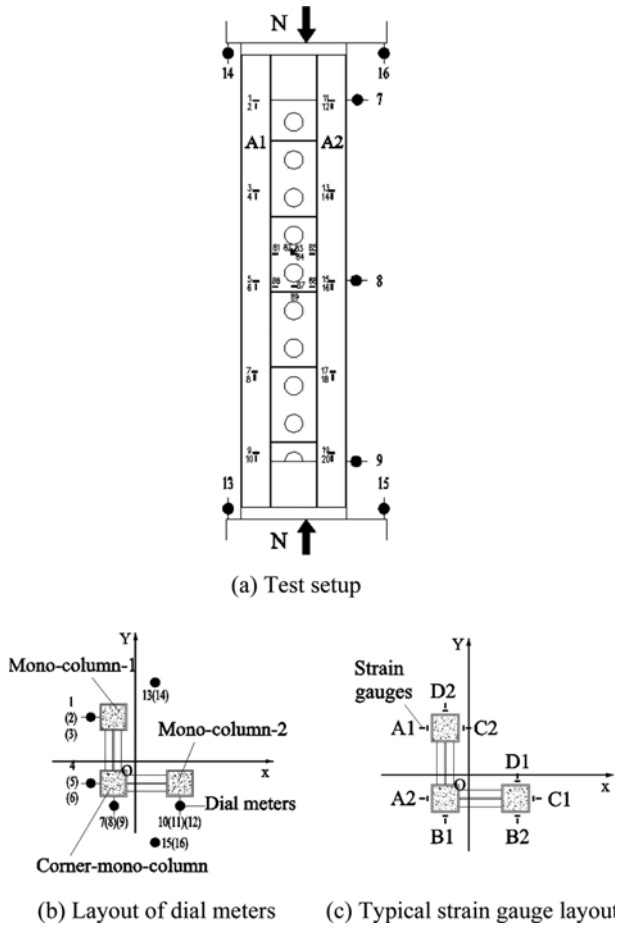

(a) Test setup

(b) Layout of dial meters (c) Typical strain gauge layout

Figure 4. Test setup and instrumentation layout.

2.3. Test setup and procedure

The test setup and instrumentation layout for the L-shaped SCFST column specimens are shown in Fig. 4. The tests were conducted using a 5,000 kN capacity Toni Pack 5000 testing machine.

The centroid of a specimen should be aligned to the midline of the testing machine when the specimen is placed in the machine. To describe the experimental results, each of the surfaces of the mono-columns were numbered as shown in Fig. 4(c). As shown in Fig. 4(b), 12 dial meters (numbers 1 to 12) were placed at the top, middle, and bottom parts of the specimens to measure lateral displacement. Two additional dial meters (numbers 14 and 16) were set at the top and another two (numbers 13 and 15) were set at the bottom of the specimens to measure vertical displacement. A total of 92 strain gauges and two strain rosettes were used in this experiment for each specimen. Strain gauges and strain rosettes were bonded to the connection plates to determine the direction of principal strains. Furthermore, 80 strain gauges were bonded to the steel tubes of each mono-column at five sections to measure the strains in the tubes along the specimen. Figure 4(c) shows the arrangement of strain gauges on one of the surfaces of a specimen, which is typical to the other four sections.

Each specimen was loaded manually at low speed. Data were logged at 20 kN intervals before yield and at 10 kN intervals after yield. To apply uniform compressive loading on the columns, two steel plates with a thickness of 40 mm each were welded to the two ends of the specimens and allowed to harden under a pre-load of 20 kN.

3. Test Results

3.1. Deformation and failure mode

The failure modes of the two specimens are shown in Fig. 5. The deformation of S-1 was not evident when the axial loading was under 1,900 kN. Axial loading began to decrease after S-1 was loaded by 1,900 kN, at which point, a small sound was heard from the deformation of the steel components. No loud sound was observed during the test. The failure mode of the specimen can be attributed to the evident buckling that occurred at one-fourth of the column height from the bottom. However, the local buckling positions of each mono-column differed, as shown in Fig. 5(a). The local buckling positions of mono-column 1 and the corner mono-column were located at their lower halves. The distance between the bottom and the failure point was approximately one-fourth of the column height. However, the local buckling position of mono-column 2 was located at the top part of the column. The deformation of the three mono-columns occurred simultaneously and developed at the same speed.

For specimen S-2, deformation was not evident until the axial loading reached 2,300 kN, at which point, a minor “hissing” sound was heard, followed by a sudden loud crash. Pronounced buckling occurred at the top part of the column, after which the load decreased rapidly. The A1, C2, and D2 areas of mono-column 1, as well as the B2, C1, and D1 areas of mono-column 2, had serious buckling at the top parts, whereas no evident deformation was observed in the corner mono-column. The failure mode is given in Fig. 5(b). Although the deformation shapes of the two mono-columns were different, which is a result of construction error and the randomness of the experiment, the failure mode of the specimen is believed to be symmetrical.

Numerous differences were noted in the experimental processes and in the failure modes between specimens S-1 and S-2. The deformation process of the specimen composed of hollow steel tubes (S-1) was characterized by a tardiness and smooth decrease of the bearing load. Meanwhile, the failure and bearing capacity decline in the column filled with concrete (S-2) occurred suddenly. In addition, the deformation shape of the mono-columns also differed. The deformation of the mono-columns of S-1 was characterized by one area (C1 or D2) of the steel tubes buckling inward and two neighboring areas buckling

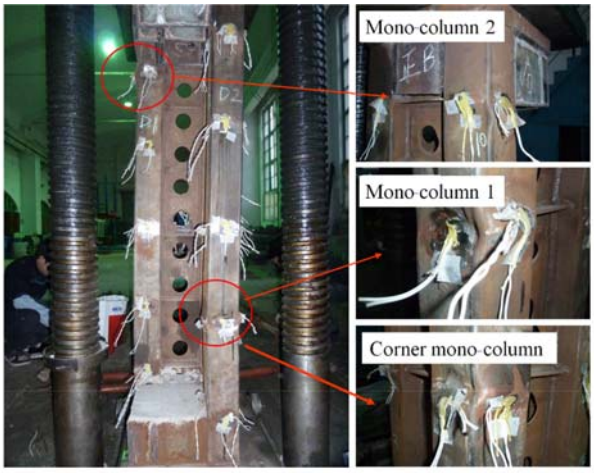

(a) S-1 (hollow steel tube)

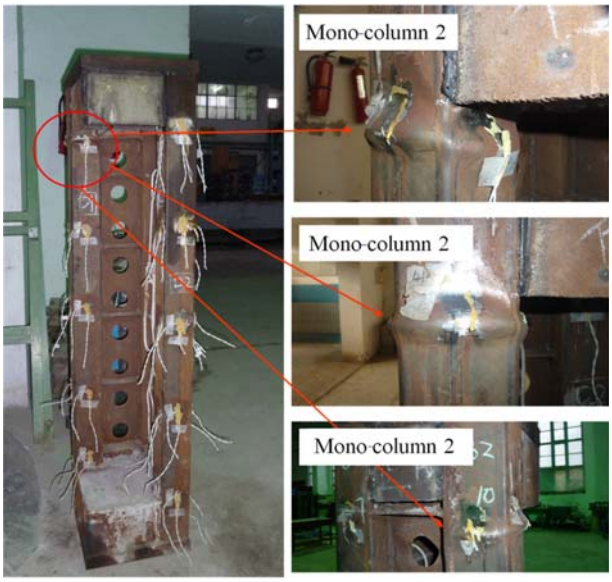

(b) S-2 (filled with concrete)

Figure 5. Failure modes.

outward. No evident buckling was found in the areas connected to the connection plates. However, the buckling of the steel tubes in S-2 was outward because the concrete core prevented the steel tubes from buckling inward.

3.2. Load-end compressive displacement

For gauging vertical deformation, two dial meters were set to measure the downward displacement of the top plate of the press machine, and another two dial meters were set to measure the upward displacement of the baseboard. The average values of the two dial meters for each plate were considered as each plate's displacement. The end compressive displacement of the specimen is the sum of the absolute values of the vertical displacements of the top plate and the baseboard. The load-end compressive displacement curves of the two specimens are shown in Fig. 6.

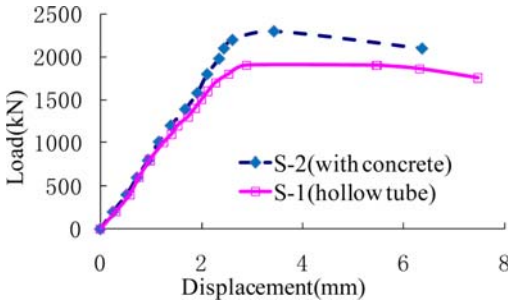

Figure 6. Load-compressive displacement curve at load-end.

The bearing capacities of the two specimens were determined according to the curves. The ultimate bearing loads of S-1 and S-2 were 1,900 and 2,300 kN respectively. The bearing capacity of the column filled with concrete increased by 21% over the column with hollow steel tubes. The same growth trend could be observed in terms of stiffness. However, a slight increase in ductility was found in S-1.

3.3. Load-lateral deformation curves

The distribution of the 12 dial meters is shown in Figs. 4(a) and (b). Dial meters 1 and 3 were used to measure the lateral displacement of the top and bottom parts of mono-column 1, and dial meter 2 was set to measure the lateral displacement of the middle part of mono-column 1. To eliminate the error of rigid displacement of the top and bottom parts, the value of dial meter 2 minus the average value of dial meters 1 and 3 was taken as the horizontal displacement of the column midpoint. The other three areas were also arranged with three dial meters, and the lateral displacements of every midpoint were determined using the same method. Figure 7 shows the axial load-lateral displacement curves for all the areas.

The curves of S-1 show that there exists out-of-plane bending in all four areas (A1, A2, B1, and B2). All four values of displacement are negative, which indicates that during the test, the movement direction of the measured points were directed away from the dial meter. This observation indicates that the column bended around the oblique axis with an angle of 135 degree from the X axis. However, the lateral deformation of S-2 differed from that of S-1. The lateral displacement values of areas A1 and A2 were positive, whereas those of B1 and B2 were negative, which indicates that the measured points of areas A1 and A2 moved toward the dial meter, whereas those of areas B1 and B2 moved away from their dial meters. Thus, specimen S-2 exhibited counterclockwise torsion.

3.4. Analysis of axial load-maximum strain curves

During the test, when the axial load reached the ultimate point, the strain gauge values began to fluctuate abruptly, resulting in a calculation error. Therefore, the

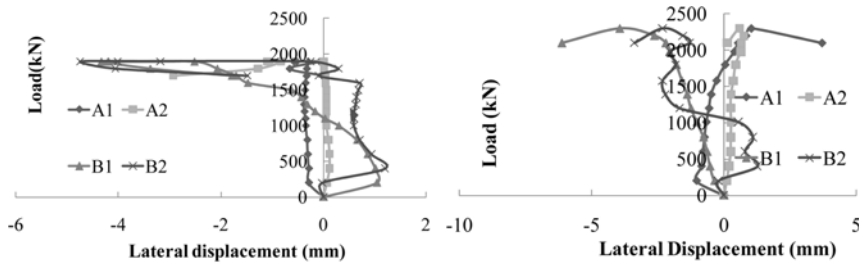

(a) S-1 (hollow steel tube) (b) S-2 (with concrete)

Figure 7. Axial load-lateral displacement curve.

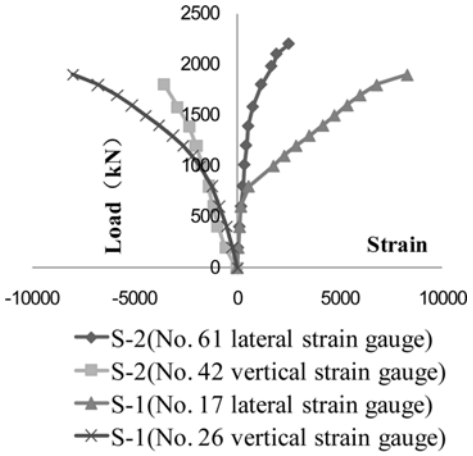

Figure 8. Axial load-maximum strain curve.

maximum strain points were determined by the strain values under 90% of the ultimate load. The load-maximum strain curves are shown in Fig. 8.

In Fig. 8, the curves with positive strains denote the lateral strain and those with negative strains denote the vertical strain because under axial loading, the vertical strain gauge was shortened whereas the lateral strain gauge was elongated. For specimen S-1, which was composed of hollow steel tubes, the maximum lateral strain point was at strain gauge 17, which was located at one-fourth of the column height from the bottom. The maximum vertical strain point of S-1 was at strain gauge 26, which was located at the middle part of the column. For specimen S-2, the maximum lateral strain point was at strain gauge 61 and the maximum vertical strain point was at strain gauge 42, both of which were located at the top part of the column. The failure mode shows that the zones with the maximum strain were the buckling areas. Specimen S-2 is composed of steel tubes filled with concrete; its top part with uncompacted concrete was significantly weaker than the middle part, which explains why the buckling areas of S-2 were located along its top part.

The comparison shows that both the stiffness and ultimate bearing capacity of S-2 are higher than those of S-1. Therefore, the inner concrete increases the axial stiffness and ultimate bearing capacity of the column.

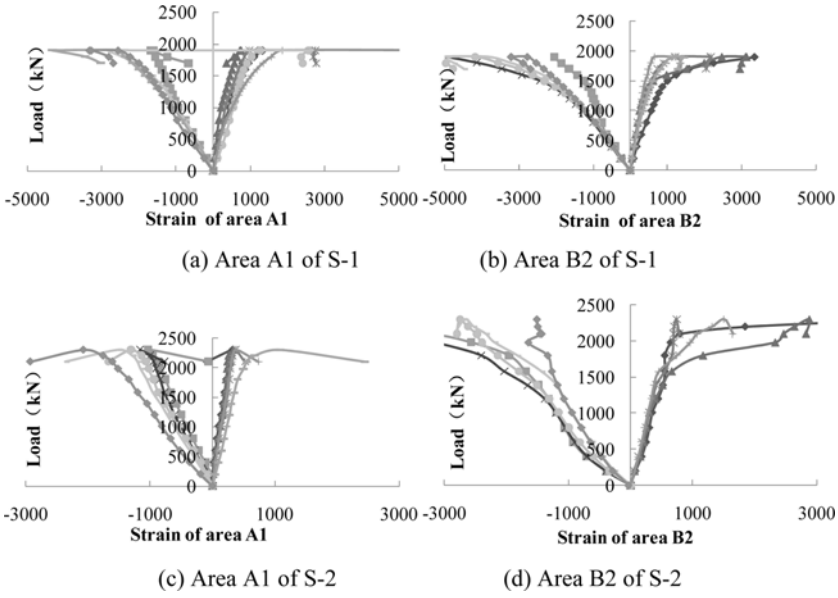

(a) Area A1 of S-1 (b) Area B2 of S-1

(c) Area A1 of S-2 (d) Area B2 of S-2

Figure 9. Vertical distributions of strain.

3.5. Vertical strain distribution

For every area of each column, five vertical strain gauges and five lateral strain gauges were set along the vertical direction. The lateral and vertical strain curves of areas A1 and B2 are given in Fig. 9 as an example. The conditions of other areas are generally identical to the example. According to the curves, the strain of each area is almost evenly distributed along the vertical direction. Therefore, if the column were axially compressed evenly, the mono-columns could work together.

3.6. Lateral strain distribution at the middle section

To study the strain of the connection plate under axial compression, the strain gauges were arranged in the middle part of the connecting plates, as shown in Fig. 4(a). At the same parts, strain gauges were also set to study the strain of steel tubes. All strain values were compared and the strain distributions on the cross section were determined. Figure 10 shows the setup of the strain gauges at the middle cross section. Two cross sections were studied: one near the stiffeners and one between the two holes without the stiffeners. For investigating the strain distribution at the second section, three load levels (30, 60, and 90% of the ultimate load) were selected. The three load levels for S-1 were set as 600, 1,200, and 1,700 kN, while those for S-2 were 600, 1,400, and 2,000 kN. The strain distributions for every load level are shown in Figs. 11 to 14.

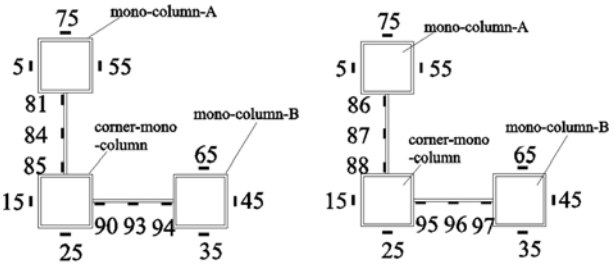

(a) Cross section without stiffeners (b) Cross section with stiffeners

Figure 10. Arrangement of strain gauges along the cross-section.

The strain distribution figures of the two specimens exhibit many common points. When the axial load was small, the strain values of the steel tubes were almost identical. However, when the load reached the ultimate load, the strain distributions of every steel tube area were no longer even. At the third load level, the strain values of the corner mono-column of S-1 were significantly greater than those of the other two mono-columns. This result indicates that column S-1 bent around the oblique axis with an angle of 135 degree from the X axis, which is in accordance with the load-lateral deformation curves.

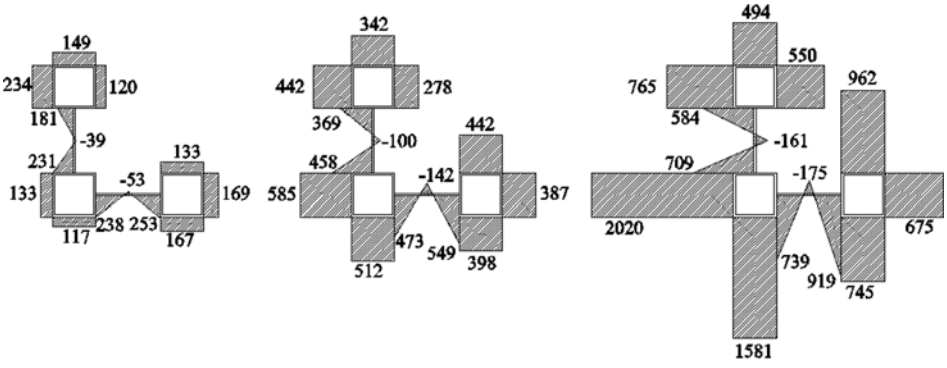

(a) 600 kN (b) 1200 kN (c) 1700 kN

Figure 11. Strain distributions at the cross section of S-1 without stiffeners.

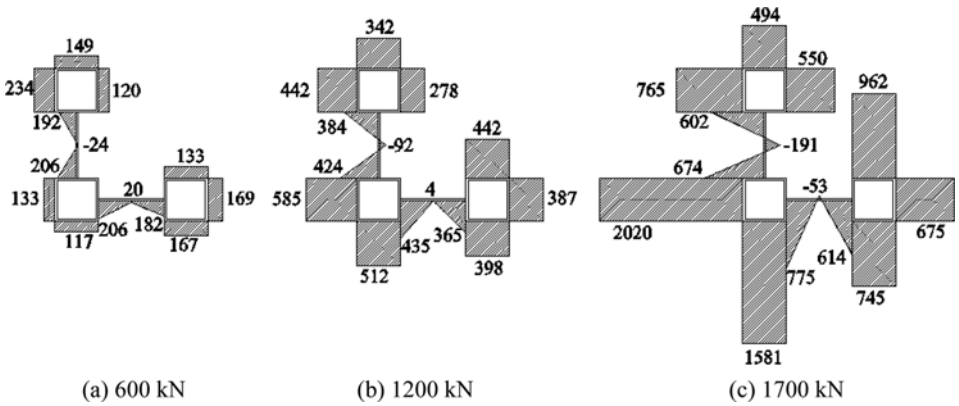

(a) 600 kN (b) 1200 kN (c) 1700 kN

Figure 12. Strain distributions at the cross section of S-1with stiffeners.

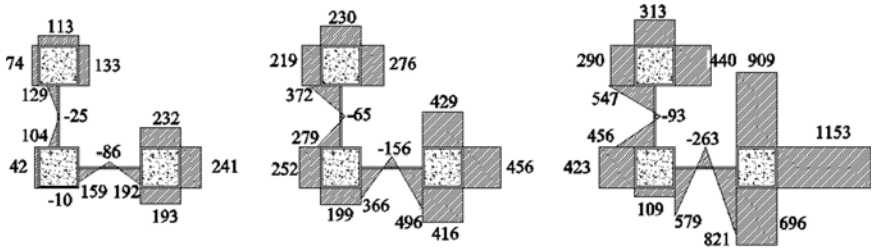

(a) 600 kN (b) 1400 kN (c) 2000 kN

Figure 13. Strain distributions at the cross section of S-2 without stiffeners.

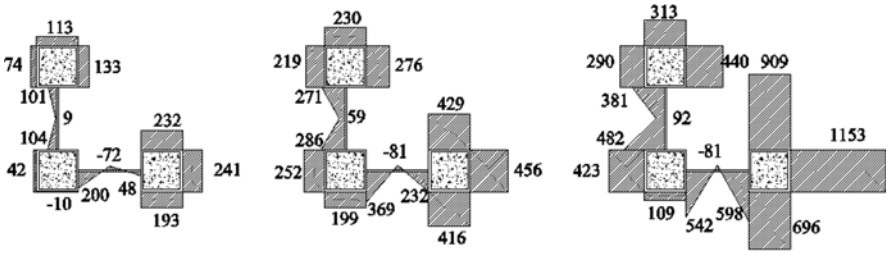

(a) 600 kN (b) 1400 kN (c) 2000 kN

Figure 14. Strain distributions at the cross section of S-2 with stiffeners.

As shown in Section 3.3, counterclockwise torsion occurred in S-2, as S-2 bent and twisted when the load reached the ultimate load.

The strain distributions on the connection plates followed a similar rule. The strains of the plates near the steel tube were significantly greater than that of the plates located in the middle parts. The differences increased with the increasing load because the axial stiffness of the connection plate is considerably lower than that of the mono-column, resulting in the increased vertical deformation of connection plates.

Meanwhile, the difference between the strains at the middle part of the connection plates and that of the connection plates near the steel tube of the area with stiffeners is lower than that of the area without the stiffeners. Therefore, the stiffeners enhance collaborative work.

Numerous differences were noted in the strain distributions of the two specimens. The maximum strain at the middle part of S-1 is 2020 μ when the axial load is 1700 kN, whereas that of S-2 is 1153 μ when the axial load is 2000 kN. Although S-1 is bearing lower axial load than S-2, the strain of S-1 is significantly larger than that of S-2.

4. Finite Element Analysis Model

A finite element model was established. The behavior of SCFST columns was rather complicated because of the nonlinearity of the inner concrete and the interaction between the concrete and the steel tubes. Therefore, established was a finite element model that could provide an efficient method to simulate the behavior of SCFST columns subjected to axial loading. The specimens were modeled and analyzed using the commercial finite element software, ANSYS.

4.1. Modeling of SCFST columns

Four main components must be modeled to simulate the behavior of SCFST columns: steel tubes, connection plates, inner-filled concrete, and the interface between the concrete and the steel tube. In addition, the selection for element type, mesh size, initial geometric deformation, boundary conditions (fixed at the top and bottom of the column), and load application is also important in simulating the SCFST columns. The modeling method has been reported in previous literature, [12] and [16]. The model of S-2 is shown in Fig. 15. The model of S-1 is identical to the model of steel shown in Fig. 15(a).

4.2. Stress distribution of steel tube, connection plate, and inner concrete

The stress-loading step curves of the specimens are shown in Fig. 16. The curves of S-1 show that the steel tube reached the ultimate strength at 0.95 s, and the connection plate buckled at 1.09 s when the stress reached 103 MPa. Likewise, the steel tube of S-2 reached the ultimate strength at 0.95 s, and the connection plate buckled at 1.2 s when the stress reached 144 MPa. According to the buckling time of the connection plate, the connection plate of S-2 buckled later than that of S-1, which demonstrates that the specimen with inner concrete has a higher bearing capacity than that without inner concrete.

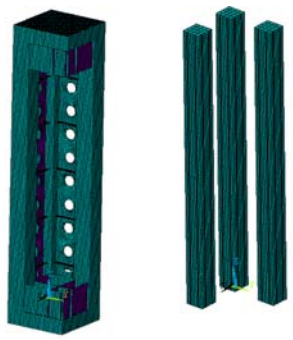

(a) Model of steel (b) Model of concrete

Figure 15. Model of CFST columns.

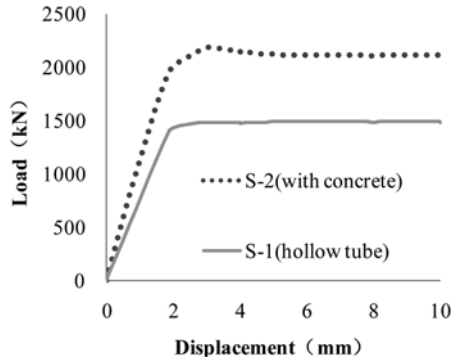

Figure 17. Load-end compressive displacement obtained by FEM.

4.3. Load-end compressive displacement

According to the finite element method (FEM) analysis, the ultimate bearing capacity of S-1 is 1396 kN and that of S-2 is 2113 kN. As shown in Fig. 17, the ultimate bearing capacity of S-2 is significantly higher than that of S-1, indicating that the inner concrete increases bearing capacity effectively.

4.4. Comparison of results

The load-end compressive displacement curves of the specimens obtained from experiments and finite element analysis are given in Fig. 18. Some differences can be observed between the test and FEM results of specimen S-1. The ultimate bearing capacity obtained by the test was higher than that obtained by FEM because the stress-strain curves of the real materials are different from those of the modeling materials, and the ultimate tensile strength of the real material is always stronger than that used in the model. However, the results for S-2 obtained by the test and FEM coincided well because the concrete used in the FEM model was free of voids, while the concrete-filled steel tube in the practical application was not compacted at the end of column, explaining the higher ultimate strength gained by FEM over the test. Given this effect, the results of finite element analysis thus agree with those of the experiment.

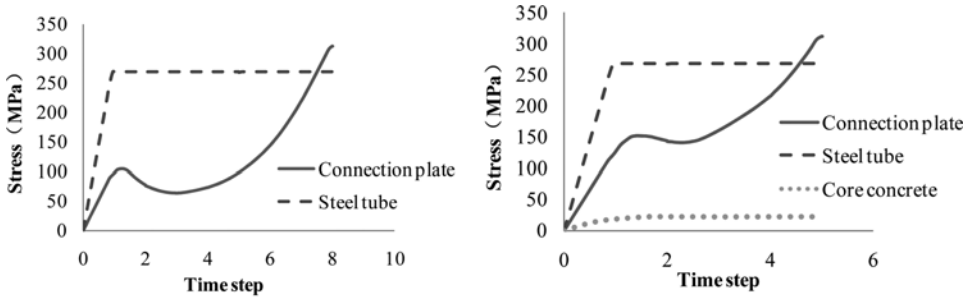

Figure 16. Stress-loading step curves.

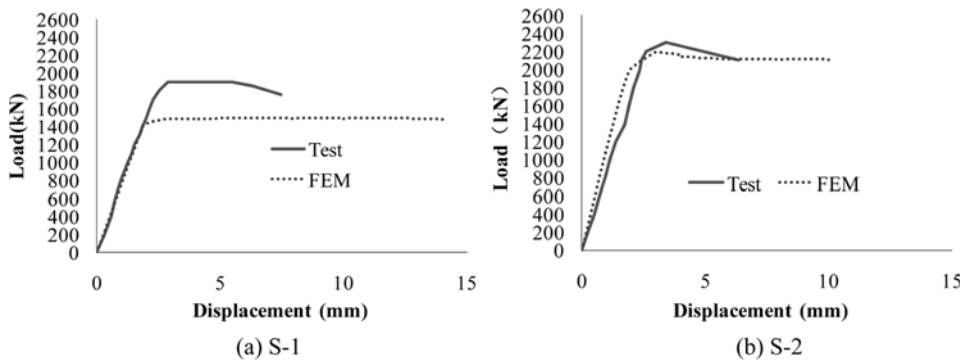

Figure 18. Comparison of load-end compressive displacement curves.

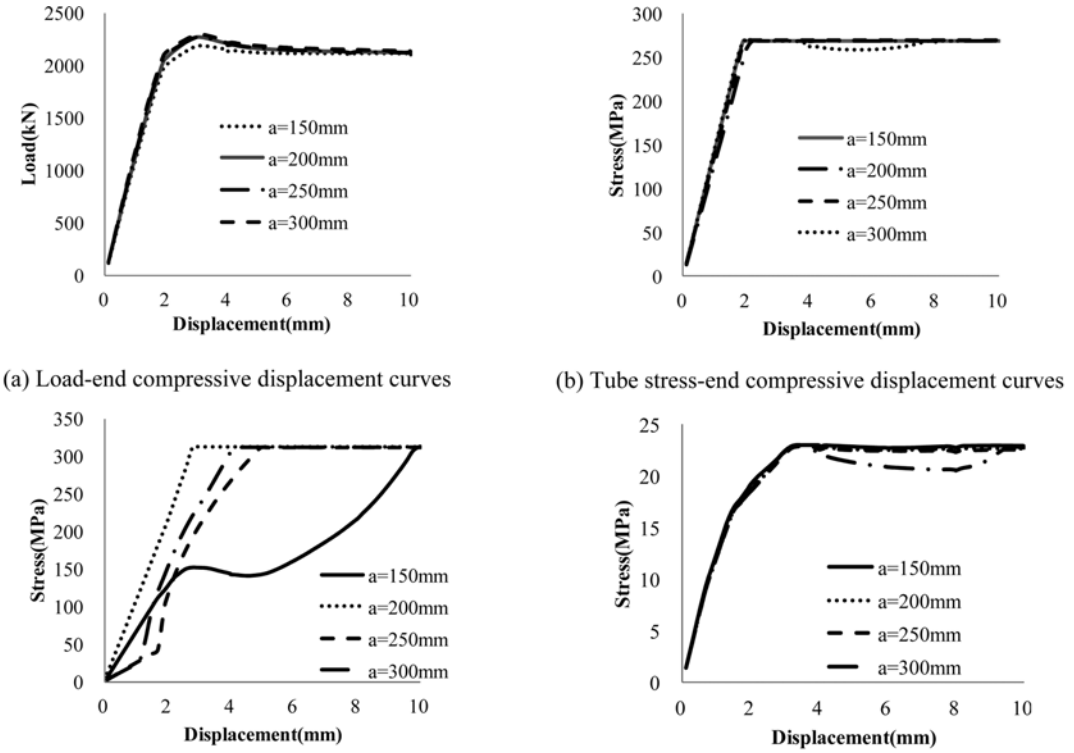

(a) Load-end compressive displacement curves

(b) Tube stress-end compressive displacement curves

(c) Plate stress-end compressive displacement curves

(d) Concrete stress-end compressive displacement curves

Figure 19. Curves of different widths of connection plates.

5. Parameter Analysis Based on Fem

According to the comparison of the test and the numerical analysis, credible results can be obtained using the FEM model. The failure mode indicates that the connection plate is a very important part of the whole special-shaped column. If the sizes of the connection plates area suitable, the mono-columns will work together well. However, we have no knowledge on designing the width and thickness of the column. Thus, the parameters of the connection plates were analyzed in this section.

5.1. Width of connection plate

Four specimens with different widths of connection plate were analyzed. The widths of connection plates (a) of these four specimens are 150, 200, 250, and 300 mm. The widths of the first specimen's connection plates were 150 mm, which are equal to that of specimen S-1 used in the test. The ultimate bearing capacity, maximum stress of steel tube, maximum stress of connection plate, and maximum stress of inner concrete were compared, the curves of which are shown in Fig. 19.

According to the curves of specimens with different widths of connection plates, the widths of the connection plates had little influence on the bearing capacity, tube stress, and concrete stress. Contrarily, the stresses of connection plates were apparently influenced by the widths of the connection plates. The specimen with the 150 mm width connection plate buckled much earlier than other specimens. According to the buckling time, the optimum width is 200 mm, meaning the optimal ratio of connection plate width to tube width is 2.

5.2. Connection plate thickness

The influence of connection plate thickness was also analyzed using the FEM model. Six specimens having connection plates of different thicknesses were calculated. The ultimate bearing capacity-end compressive displacement curves of these specimens are shown in Fig. 20(a). The connection plate thickness had an apparent influence on the ultimate bearing capacity. An increase in connection plate thickness translated to an increase in the bearing capacity. As shown in Fig. 20(b), when the thickness increases from 3 to 6 mm, the ultimate bearing capacity increases to 172 kN; however, as the thickness increases, the increment of bearing capacity decreases. According to these conditions, the optimal thickness was considered to be 6 mm, meaning the optimal ratio of connection plate thickness to tube thickness is approximately 1.5.

6. Conclusions

The behavior of SCFST columns subjected to axial load was experimentally investigated. The effects of the inner concrete of SCFST columns were studied. The experimental results were compared with those from

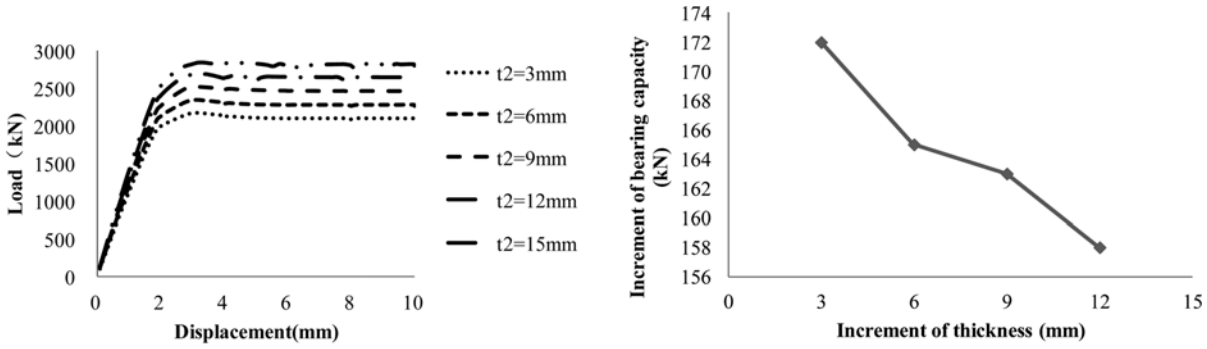

(a) Load-end compressive displacement curves

(b) Increment of bearing capacity according to the connection plate thickness curve

Figure 20. Curves of different thicknesses of connection plates.

finite element analysis. The conclusions can be drawn as follows:

(1) The failure of SCFST columns subjected to axial load was caused by the local buckling of mono-columns. The failure mode of the specimen composed of hollow steel tubes was characterized by the inward buckling of one area (C1 or D2) of the steel tube and by the outward buckling of neighboring areas. Meanwhile, the failure of the specimen filled with concrete was caused by the outward buckling of steel tubes resulting from the support extended by the inner concrete. Meanwhile, the load-lateral deformation curves and the strain distributions indicate that S-1 bent and that S-2 bent and twisted.

(2) The ultimate bearing capacity of S-2 is 21% higher than that of S-1, and the stiffness of S-2 is enhanced by the inner concrete. However, the declining slope of the load-deformation curve of S-2 is steeper, indicating that ductility decreases.

(3) According to the vertical and lateral strain distributions, the columns were axially compressed evenly and the mono-columns could work together. Moreover, the stiffeners on the connection plates could prevent the connection plates from buckling.

(4) The results obtained by finite element analysis agreed with those obtained by the test. Thus, finite element analysis can effectively simulate the behavior of SCFST columns.

(5) The influence of connection plate size on the bearing capacity was analyzed using the FEM model. The optimal ratios of connection plate sizes to steel tube sizes were proposed. The best ratio of connection plate width to tube width is 2, and the optimal ratio of connection plate thickness and that of a tube is approximately 1.5.

Acknowledgments

This work is sponsored by the National Natural Science Foundation of China (Grant no. NSFC51308387).

Nomenclature

a	Distance between mono-columns
b	Width of mono-column
t_1	Thickness of steel tube
t_2	Thickness of connection plate
t	Thickness of steel in material tests
A_y	Steel area of mono-column
A_c	Concrete area of mono-column
l	Length of column
N	Axial compression applied to specimen
f_y	Yield strength
f_u	Ultimate strength
ε_y	Yield strain
f_{cu}	Axial compressive strength of concrete cube with a width of 150 mm
f_c	Axial compressive strength of 150×150×300 mm concrete cuboids
ε_0	Value of lateral strain gauge
ε_{90}	Value of vertical strain gauge
ε_{45}	Value of strain gauge at 45°
ε_x, ε_y	Normal strains
γ_{xy}	Shearing strain
ε_1, ε_2	Principal strain
θ_p	Angle between the first principal and the x-axis

References

Chen, Z., Li, Z., Rong, B., and Liu, X. (2006). "Experiment of axial compression bearing capacity for crisscross section special-shaped column composed of concrete-filled square steel tubes." *Journal of TianJin University*, 39(11), pp. 1275-1282 (in Chinese).

Chen, Z. H., Rong, B., and Fafitis, A. (2009). "Axial compression stability of a crisscross section column composed of concrete-filled square steel tubes." *Journal of Mechanic of Materials and Structures*, 4(10), pp. 1787-1799.

Chen, Z. H., Zhou, T., and Wang, X. D. (2011). "Application of special shaped column composed of concrete-filled

steel tubes." *Advanced Materials Research*, 163-167, pp. 196-199.

Cheng, T. and Thomas, H. (1989). "T-shaped reinforced concrete members under biaxial bending and axial compression." *ACI Structural Journal*, 86(4), pp. 2576-2595.

Dundar, C. and Sahin, B. (1993). "Arbitrarily shaped reinforced concrete members subjected to biaxial bending and axial load." *Computers & Structures*, 49(4), pp. 643-662.

Gao, D. X., Ke, J., and Wang, L. H. (2005). "Seismic behavior analysis of special-shaped column frame structure." *Journal of Xi'an University of Technology*, 21(3), pp. 285-288 (in Chinese).

Guo, L. H., Wang, Y. Y., and Zhang, S. M. (2012). "Experimental study of concrete-filled rectangular HSS columns subjected to biaxial bending." *Advances in Structural Engineering*, 15(8), pp. 1329-1344.

Han, L. H. (2002). "Tests on stub columns of concrete-filled RHS sections." *Journal of Constructional Steel Research*, 58(3), pp. 353-372.

Han, L. H., Liu, W., and Yang, Y. F. (2008). "Behavior of concrete-filled steel tubular stub columns subjected to axially local compression." *Journal of Constructional Steel Research*, 64, pp. 377-387.

Joaquin, M. (1979). "Design aids for L-shaped reinforced concrete columns." *ACI Structural Journal*, 76(49), pp. 1197-1216.

Mallikarjuna and Mahadevappa, P. (1992). "Computer aided analysis of reinforced concrete columns subjected to axial compression and bending. Part I: L-shaped sections." *Computers & Structures,* 44(5), pp. 1121-1138.

Shen, Z. Y., Lei, M., Li, Y. Q., Lin, Z. Y., and Luo, J. H. (2013). "Experimental study on seismic behavior of concrete-filled L-shaped steel tube columns." *Advances in Structural Engineering*, 16(7), pp. 1235-1247.

Yang, Y., Yang, H., and Zhang, S. (2010). "Compressive behavior of T-shaped concrete filled steel tubular columns." *International Journal of Steel Structures*, 10(4), pp. 419-430.

Zhou, T., Chen, Z. H., and Liu, H. B. (2010). "Seismic behavior of special shaped column composed of concrete filled steel tubes." *Journal of Constructional Steel Research*, 75, pp. 131-141.